Published in final edited form as:
Hum Mol Genet. 1997 July ; 6(7): 1091–1098.

Identification of mutations in two major mRNA isoforms of the Chediak–Higashi syndrome gene in human and mouse

Maria D. F. S. Barbosa[1,+], **Franck J. Barrat**[2,+], **Velizar T. Tchernev**[1,+], **Quan A. Nguyen**[1], **Vishnu S. Mishra**[1], **Steven D. Colman**[3], **Elodie Pastural**[2], **Rémi Dufourcq-Lagelouse**[2], **Alain Fischer**[2], **Randall F. Holcombe**[5], **Margaret R. Wallace**[3], **Stephen J. Brandt**[4], **Geneviève de Saint Basile**[2,*], and **Stephen F. Kingsmore**[1,*]

[1] Departments of Medicine, [1]Pathology, Center for Mammalian Genetics, University of Florida, Gainesville, FL 32610-0221, USA

[2] INSERM U 429, Hopital Necker-Enfants Malades, 75743 Paris, Cedex 15, France

[3] Department of Pediatrics, Center for Mammalian Genetics, University of Florida, Gainesville, FL 32610-0221, USA

[4] Departments of Medicine and Cell Biology, Vanderbilt University, Nashville, TN 37232, USA

[5] Departments of Medicine, Microbiology and Immunology, Louisiana State University Medical Center, Shreveport, LA 33932, USA

Abstract

Chediak–Higashi syndrome is an autosomal recessive, immune deficiency disorder of human (*CHS*) and mouse (beige, *bg*) that is characterized by abnormal intracellular protein transport to, and from, the lysosome. Recent reports have described the identification of homologous genes that are mutated in human *CHS* and *bg* mice. Here we report the sequences of two major mRNA isoforms of the *CHS* gene in human and mouse. These isoforms differ both in size and in sequence at the 3′ end of their coding domains, with the smaller isoform (~5.8 kb) arising from incomplete splicing and reading through an intron. These mRNAs also differ in tissue distribution of transcription and in predicted biological properties. Novel mutations were identified within the region of the coding domain common to both isoforms in three CHS patients: C→T transitions that generated stop codons (R50X and Q1029X) were found in two patients, and a novel frame-shift mutation (deletion of nucleotides 3073 and 3074 of the coding domain) was found in a third. Northern blots of lymphoblastoid mRNA from CHS patients revealed loss of the largest transcript (~13.5 kb) in two of seven CHS patients, while the small mRNA was undiminished in abundance. These results suggest that the small isoform alone cannot complement Chediak–Higashi syndrome.

INTRODUCTION

Chediak–Higashi syndrome (CHS) is an autosomal recessive, immune deficiency disease that maps to human chromosome (Chr) 1q42–q43 (1–3). Affected individuals have giant, perinuclear lysosomes, defective granulocyte, natural killer (NK) and cytolytic T-cell function, and die prematurely of infection or malignancy (4–10). CHS patients also exhibit partial oculocutaneous albinism, platelet storage pool deficiency and late neurologic defects such as peripheral neuropathy and ataxia (11–15). Recently, it has been demonstrated that intracellular

*To whom correspondence should be addressed. S.F.K. Tel: +1 352 392 8600; Fax: +1 352 392 8483; kingsmore@cmg.health.ufl.edu or G.S.B. Tel: +331 44 49 5080; Fax: +331 42 73 0640; sbasile@necker.fr.
[+]These authors contributed equally to this work

protein transport to, and from, the lysosome is disordered in CHS (10,16–18). The defects in trafficking of secretory lysosomes of granular cells (leukocytes, melanocytes, megakaryocytes and cerebellar Purkinje cells) provide a unifying hypothesis that explains the diverse clinical features of CHS (19), and suggest that the CHS gene regulates intracellular protein transport to, and from, the lysosome.

As an antecedent to identification of the human *CHS* gene, two groups positionally cloned the homologous mouse mutation, beige (*bg*) (20,21). The clinical and pathologic features of *CHS* and *bg* are very similar, and *bg* maps on proximal mouse Chr 13 within a linkage group conserved with human Chr 1q42–q43 (the position of the CHS locus) (1–3,22–24). Subsequently, the human homolog of the *bg* gene was mapped to Chr 1q43, and found to be mutated in three CHS patients(20,25). There has been some ambiguity, however, in the literature about the exact structure of the mouse Chediak–Higashi syndrome (*bg*) gene (designated *Lyst*) (20,21). We reported a novel mouse cDNA from a *bg* critical region yeast artificial chromosome (YAC) that was mutated in *bg* mice (20). Simultaneously, another group published a partial cDNA sequence that had been isolated from the same YAC clone (21). The latter was mutated in two other *bg* alleles, but differed in sequence from the former. In the present report, this discrepancy was explained by the demonstration that each of the previously reported *bg* gene sequences are derived from a single gene with alternatively spliced mRNAs. We also report the sequences of two major isoforms of the *CHS* gene in human. These isoforms arise in mouse and human as a result of incomplete mRNA splicing and differ in pattern of expression and predicted biological properties.

RESULTS

Incomplete splicing generates two mRNA isoforms of the mouse *bg* gene

The existence of more than one mRNA isoform of the mouse *bg* gene (designated *Lyst*) had been suggested both by Northern blot analysis and by *Lyst* cDNA sequences that differed at their 3′ end (20,24). Mouse *Lyst* mRNA isoforms were therefore sought by anchored, nested PCR (3′RACE-PCR). Two fragments (1.25 and 2 kb) were amplified from mouse spleen cDNA using this technique. The 1.25 kb clone contained the 3′ end of the previously described 5893 bp *Lyst* cDNA that corresponds to a small mRNA isoform (Lyst-II) (20). The 5′ end of the 2 kb clone, however, contained sequence derived from the *Lyst*-II cDNA, while the 3′ end sequence was from the largest isoform of the *bg* gene (*Lyst*-I, previously called BG) (24). Reverse transcription and PCR (RT-PCR) confirmed that nucleotides 1–4706 of *Lyst* are common to both mRNA isoforms (Fig. 1A). The large isoform cDNA that contains the entire coding domain was assembled from nucleotides 1–4706 of *Lyst*, the 2 kb 3′RACE-PCR clone, and 6824 nucleotides of BG cDNA. This 11 817 bp cDNA sequence (*Lyst*-I, GenBank accession no. U70015) corresponds to the largest mRNA observed in Northern blots (20). This 11.8 kb cDNA, however, is truncated at both the 5′ end of the 5′-untranslated region (UTR) and at the 3′ end of the 3′ UTR, and thus is smaller than the largest mRNA observed on mouse Northern blots (~12–13 kb) (20).

Analysis of a P1 genomic clone (number 8592) (26) containing the entire *bg* gene revealed that the 11 817 bp *Lyst*-I cDNA results when splicing occurs from *Lyst* exon σ (containing nucleotide 4706) to downstream exon τ (Fig. 1A and B). In contrast, incomplete splicing and reading through intron σ′ interposed between exons σ and τ yields the truncated *Lyst*-II isoform, of length 5893 bp cDNA (*Lyst*-II, Fig. 1A and B, GenBank accession No. L77884). *Lyst* intron σ′ encodes 37 in-frame amino acids followed by a stop codon and a polyadenylation signal. *Lyst*-II corresponds to one of several smaller mRNAs observed on Northern blots (20). Full-length cDNAs corresponding to the *Lyst*-I and *Lyst*-II isoforms were both amplified readily from mouse bone marrow RNA by RT-PCR (data not shown). The putative Lyst-I and Lyst-II proteins are of relative molecular mass 425 287 (M_r 425 kDa) and M_r 172.5 kDa, respectively.

Sequences of two isoforms of the human Chediak–Higashi syndrome gene

cDNAs corresponding to the human homolog of the largest mRNA isoform of the *bg* gene were obtained by identification of human expressed sequence tags (ESTs) similar in sequence to mouse *Lyst*-I by database searches (GenBank accession Nos L77889, W26957 and H51623) (Fig. 1C). Intervening cDNA sequences were isolated using RT-PCR, and a partial human cDNA sequence (GenBank accession No. U70064; 7.1 kb) was assembled by alignment of these clones with the largest mouse *bg* gene cDNA (Fig. 1C). The predicted human and mouse peptides shared 82% amino acid identity over 1990 amino acids. The predicted human amino acid sequence contains a six amino acid insertion relative to that of mouse at residue 1039. While this paper was being reviewed, another group published the complete sequence of the human CHS cDNA (25). Our partial cDNA sequence differs in four nucleotides and three predicted amino acids from the latter (25). This 13.5 kb cDNA sequence corresponds to the largest mRNA observed on Northern blots of human tissues (*CHS*-I, legend of Fig. 2) (20). These Northern blots also demonstrated the existence of a smaller human transcript (~4.5 kb) that was similar in size to the small mouse *Lyst* mRNA, and that appeared to differ in distribution of expression in human tissues from the large isoform (20). Assuming that the genomic derivation of the human small isoform might be the same as the mouse small isoform, the 3′ end of the human small isoform was identified by cloning human intron σ′ using PCR of human genomic DNA with primers derived from exon σ and intron σ′. As in the mouse, the sequence of the 5′ end of human intron σ′ contained 17 codons in-frame with exon σ, followed by a stop codon (*CHS*-II, legend of Fig. 2). cDNA corresponding to this human short isoform was amplified from human peripheral blood RNA by RT-PCR with primers from a 5′ exon and intron σ′, indicating that this intron was indeed present in *CHS*-II mRNA (data not shown). Nucleotides 1–5905 of human small and long isoform cDNAs are identical, and are followed either by intron σ′ sequence in the short isoform (GenBank accession No. U84744), or by exon τ, etc. in the long isoform (Fig. 2 legend). The predicted intron-encoded aminotermini of the mouse and human short isoform peptides shared 65% identity.

Additional splicing complexity of small *CHS* isoforms exists: exon α, and/or exon β, and/or exon γ also can be alternatively spliced, and are absent in small *CHS* isoform mRNAs of ~3.5, 4.5 and 5.5 kb, that correspond to additional bands observed on human Northern blots (20).

The only significant sequence similarity of the human short isoform to known proteins was with the stathmin family (20). Identity with mouse Lyst-II in this region (amino acids 376–540) was 92% (and similarity was 99%) (Fig. 4).

Expression of the long and short isoform mRNAs in human tissues

Analysis of Northern blots of mouse mRNA had suggested that the relative abundance of the mouse large and small transcripts differed from tissue to tissue (20). The relative abundance of mRNA isoforms of the homologous human gene in human tissues at different developmental stages was examined by sequential hybridization of a poly(A)$^+$ RNA dot-blot with several cDNA probes. The quantity of poly(A)$^+$ RNA loaded on the blot was normalized to eight housekeeping genes (phospholipase, ribosomal protein S9, tubulin, a highly basic 23 kDa protein, glyceraldehyde-3-phosphate dehydrogenase, hypoxanthine guanine phosphoribosil transferase, β-actin and ubiquitin).

Using a probe that hybridized only to the largest mRNA isoform on Northern blots (20), transcripts were most abundant in thymus (adult and fetal), peripheral blood leukocytes, bone marrow and several regions of the adult brain (Fig. 2). However, the largest mRNA isoform was not detected in fetal brain. There was also negligible transcription of this isoform in heart, lung, kidney and liver in all developmental stages.

A somewhat different pattern of relative expression was evident upon rehybridization of the blot with a probe derived from the 5′ end of the coding domain of *CHS* (Fig. 2), a region that hybridized to all mRNA isoforms on Northern blots (20). Consistent with the transcription pattern of the largest isoform, this probe detected abundant expression in peripheral blood leukocytes, thymus (adult and fetal) and bone marrow, but negligible expression in skeletal muscle. However, several tissues with abundant large isoform transcripts exhibited considerably less relative expression with the 5′ probe, including most regions of the adult brain, fetal and adult thymus, and spleen. Furthermore, several tissues with negligible large isoform relative transcription exhibited increased relative expression with the 5′ probe, including adult and fetal heart, kidney, liver, and lung, and adult aorta, thyroid gland, salivary gland and appendix, and fetal brain.

Mutation analysis

As an initial screen for mutations in CHS patients, we analyzed Northern blots of poly(A)$^+$ RNA from CHS patients. The largest mRNA species (~13 kb) was greatly reduced in abundance or absent in lymphoblastoid mRNA of patients P1 and P3, respectively (Fig. 3A), while the smaller transcript (~4.4 kb) was both present and undiminished in abundance in all three patients. While the selective loss of the larger transcript in these two patients cannot be excluded definitively, rehybridization of this blot with an actin probe suggested that absence of the larger transcript was not due to uneven gel loading or RNA degradation (data not shown). Fibroblast poly(A)$^+$ RNA from three other CHS patients (369, 371 and 373) showed a moderate reduction in the ~13 kb mRNA (51–60% of control by densitometry), while the ~4.4 kb mRNA was essentially unaltered in abundance (103–147% of control) (data not shown).

Single-strand conformation polymorphism (SSCP) analysis was undertaken using cDNA samples derived from lymphoblastoid or fibroblast cells lines from CHS patients. Anomalous bands were detected in PCR products from the 5′ end of the open reading frame (ORF) in two unrelated CHS patients (371 and 373) different from those with probable selective loss of the larger transcript on Northern blots (Fig. 3B). Sequence analysis identified a C→T substitution at nucleotide 148 of the coding domain in patient 373 (Fig. 3C). Four of nine cDNA clones derived from patient 373 contained this mutation. Restriction enzyme digestion confirmed this mutation: *Taq*I digestion of cDNA (nucleotides 520–808) showed loss of this restriction site in patient 373 to be heterozygous (data not shown). The C→T substitution creates a stop codon at amino acid 50 (R50X). The mutation in patient 373 occurs within a CpG dinucleotide, which represents a common hotspot for mutations when methylated.

Patient 371 had been shown previously to have a frameshift mutation with a G insertion at nucleotide 118 of the coding domain (Fig. 3C) (20). While analysis of genomic DNA had shown patient 371 to be heterozygous for this mutation(24), each of five cDNA clones isolated from lymphoblasts of this patient contained the insertional mutation. Allele-specific oligonucleotide (ASO) hybridization of cDNA from this patient failed to detect a signal with an oligonucleotide corresponding to the normal allele, suggesting that the patient is transcriptionally hemizygous for the G insertion mutation. Alternatively, the lack of ASO hybridization may reflect a base mismatch (such as a polymorphism) within the patient's cDNA.

Novel mutations were identified in two other CHS patients: a homozygous C→T substitution at nucleotide 3085 of the coding domain that created a stop codon at amino acid 1029 (Q1029X) was found in patient 370, and a heterozygous frameshift mutation was found in patient 369. Nucleotides 3073 and 3074 of the coding domain were deleted in two of five cDNA clones isolated from the latter patient. This deletion results in a frameshift at codon 1026 and termination at codon 1030.

Despite mutation analysis of >6 kb of ORF, the mutations in CHS patients P1 and P3 (that appear to have selective loss of the larger transcript on Northern blots) have not been identified.

Lymphoblasts from all of these patients (369, 370, 371, 373, P1 and P3) contain the giant perinuclear lysosomal vesicles that are the hallmark of CHS. Patients 369, 370 and 371 had typical clinical presentations of CHS, with recurrent childhood infections and oculocutaneous albinism. The parents of patients 369 and 370 are known not to have been consanguinous. In contrast, the clinical course of patient 373 was milder: This patient has not had systemic infections and remains alive at age 37. Patient 373 does, however, have hypopigmented hair and irides as well as peripheral neuropathy.

DISCUSSION

We have demonstrated here that each of the previously reported *bg* gene sequences (20,21) are derived from a single gene with alternatively spliced mRNAs. The previously reported sequences are derived from non-overlapping parts of two *Lyst* mRNA isoforms with different predicted C-terminal regions. By sequencing RT-PCR products, we have shown that nucleotides 1–4706 of *Lyst* also represent the previously undetermined 5′ region of the largest *Lyst* isoform. Alternative splicing at nucleotide 4706 results in *bg* gene isoforms that contain different 3′ regions. Splicing from exon σ (containing nucleotide 4706) to exon τ results in an ~12 kb mRNA (*Lyst*-I) that corresponds to the largest band observed on Northern blots. Incomplete splicing at nucleotide 4706 results in a 5893 bp cDNA (*Lyst*-II) that contains intron-derived sequence at the 3′ end. *Lyst*-II corresponds to a smaller mRNA observed on Northern blots (20). While several other genes generate an alternative C-terminus by incomplete splicing (27–31), the *bg* gene is unique in that the predicted structures of the two C-termini are quite different. The C-terminus of Lyst-I contains a ‘WD’-repeat domain that is similar to the β-subunit of heterotrimeric G proteins and which may assume a propeller-like secondary structure (32). This domain is absent in Lyst-II.

Northern blots of human tissues had suggested that transcription of the homologous human gene, *CHS*, has a similar complexity to the mouse (20). We recently identified two human ESTs homologous to mouse *Lyst* and described a mutation in one of these in a CHS patient (20). Subsequently, another group published the cDNA sequence of the largest *CHS* isoform, and identified mutations in this gene in two additional patients with CHS (25). Here we have described the identification of a second isoform of the human *CHS* gene. This mRNA encodes a protein of 1531 amino acids that is homologous to mouse *Lyst*-II. Like the latter, this human mRNA arises from incomplete splicing and retention of a transcribed intron that encodes the C-terminus of the predicted CHS protein. The mouse and human codons unique to this short isoform share 65% amino acid identity. The stop codon, however, is not conserved precisely between the human and mouse short isoforms. While mouse Lyst-II is predicted to contain a C-terminal prenylation motif (CYSP), translation of human short isoform is predicted to terminate 22 codons earlier and to lack this motif.

However, the other predicted structural features of the human short isoform were conserved with mouse. The most notable of these was a region similar in sequence to stathmin (amino acids 376–540) (20). While the mouse and human *CHS* genes had an overall amino acid identity of 81%, identity in the stathmin-like domain was 92% (and similarity was 99%) (Fig. 4). Stathmin is a coiled-coil phosphoprotein that regulates microtubule polymerization in a phosphorylation-dependent manner, and acts as a relay for intracellular signal transduction (33–35). This region of the *CHS* gene may encode a coiled-coil protein interaction domain and may regulate microtubule-mediated lysosome trafficking. Intriguingly, a defect in microtubule dynamics has been documented previously in CHS (36) and intact microtubules are required for maintenance of lysosomal morphology and trafficking (37–40).

Comparison of the relative abundance of *CHS* gene transcripts in human tissues at different developmental stages revealed an overlapping but distinct pattern of expression (Fig. 2). A quantitative estimate of the relative expression of the smaller mRNA isoforms was obtained by comparing the relative hybridization intensity obtained with a probe specific for the large isoform with that obtained with a probe that hybridizes to all *CHS* transcripts. Large isoform transcripts predominated in thymus, fetal thymus, spleen and brain (with the exception of amygdala, occipital lobe, putamen and pituitary gland). Large and small mRNA transcripts were abundant in the latter brain tissues, peripheral blood leukocytes and bone marrow. However, in several tissues, only the small isoforms were expressed, including heart, fetal heart, aorta, thyroid gland, salivary gland, kidney, liver, fetal liver, appendix, lung, fetal lung and fetal brain. The developmental pattern of mRNA isoform expression in brain was particularly interesting, since only the small isoforms were expressed in fetal brain, whereas the largest isoform predominated in many regions of the adult brain.

Novel mutations were identified within the coding domain of the *CHS* gene in three CHS patients (Table 1). The genetic lesions in two CHS patients (370 and 373) were C→T substitutions that resulted in premature termination (Q1029X and R50X, respectively). Another patient had a frameshift mutation. This patient was heterozygous for a dinucleotide deletion that results in premature termination at codon 1030. Interestingly, all *bg* and *CHS* mutations identified to date are predicted to result in the production of either truncated or absent proteins (20,21,25). Unlike Fanconi anemia, type C, there does not appear to be a correlation between the length of the truncated proteins (which may or may not be stable) with clinical features or disease severity in CHS patients (41). However, until the other mutant allele in the compound heterozygote patients is identified, and the exact effects of each mutation at the protein level are characterized, such correlation is imprecise.

An important question that remains to be answered definitively is which transcripts are biologically relevant in regulating lysosomal trafficking and in preventing CHS. The distribution of expression of mRNA isoforms in human tissues was consistent with the pattern of clinical features observed in CHS patients: transcripts were most abundant in peripheral blood leukocytes, bone marrow, thymus, lymph node, spleen and brain, and common clinical features among CHS patients are immune deficiency, platelet storage pool deficiency, neurologic manifestations and albinism. Northern blots demonstrated an ~13 kb mRNA (corresponding to the largest isoform) to be severely reduced in abundance in two CHS patients. A 4.4 kb band (corresponding to a smaller isoform), however, was present in mRNA from these patients in normal abundance. These results suggest that in some patients CHS results from loss of the protein encoded by the largest isoform. All of the mutations identified in CHS patients to date are within the region of the coding domain that is common to all isoforms (20,25). However, the mouse bg^{8J} mutation results in the generation of a premature stop codon in *Lyst*-I that is unlikely to affect *Lyst*-II mRNA processing (21). Together, these results suggest that defects in the full-length mRNA alone can elicit CHS and that expression of the smaller isoform alone cannot compensate for loss of the largest isoform.

MATERIALS AND METHODS

Cloning of human *CHS* cDNAs

Segments of the human *CHS* sequence were obtained by an anchored, nested PCR (5′RACE-PCR) using liver cDNA as a template (Clontech Laboratories, Palo Alto, CA), by RT-PCR using total RNA and by sequencing of human ESTs similar in sequence to mouse *Lyst*. For the 5′RACE-PCR, two nested primers were used that were derived from a human EST (GenBank accession No. W26957) and had the following nucleotide sequences: 5′-CCAAGATGAAAGCAGCCGATGGGGAAAACT-3′ and 5′-TCAGCCTCTTTCTTGCTCCGTGAAACTGCT-3′. For RT-PCR experiments, total RNA

was prepared from the promyelocytic HL-60 cell line. RT-PCR was performed with Expand polymerase (Boehringer Mannheim, Meylan, France) with the following primer pairs: 5′-AGTTTATGAGTCCAAATGAT-3′ and 5′-GAATGATGAAGTTGCTCTGA-3′ (bp 490–2034); 5′-CAGCAGTTCTTCAGATGGA-3′ and 5′-ATCTTTCTGTTGTTCCCCTA-3′ (bp 1891–3050); and 5′-TAGGGGAGCAACAGAAAGAT-3′ and 5′-GCTCATAGTAGTATCACTTT-3′ (bp 3320–4722). The primers used to amplify the cDNA between base pairs 1891 and 3050 were derived from the mouse *Lyst* sequence (20). Human primers were designed from the sequence of the PCR product (1159 bp) and used to amplify the flanking sequences. Human *CHS* intron σ′ was PCR amplified from human genomic DNA (100 ng) with the primers 5′-CCGCTCGAGTAGGATCTTTAAGGTGAATAAC-3′ and 5′-GTGATACTACTATGAGCCCTTCACAGTATC-3′. PCR conditions were: 94°C for 1 min, then 32 cycles of 94°C for 15 s, 63°C for 20 s and 72°C for 30 s, followed by 10 min at 72°C.

Long-range PCR of mouse *Lyst* cDNA isoforms

Total cellular RNA was isolated from mouse bone marrow cells with Trizol (Life Technologies Inc., Bethesda, MD). Five μg of RNA was reverse transcribed using Superscript reverse transcriptase (Life Technologies Inc.), with first strand cDNA synthesis priming by an oligo (dT) primer and a gene-specific primer (5′-CACAGTCATGGGACTGCTAA-3′) for *Lyst*-I and *Lyst*-II, respectively. One μl of cDNA was used as template for PCR amplification using KlenTaq DNA polymerase (Clontech, Palo Alto, CA). PCR conditions were: 94°C for 1 min, then 30 cycles of 94°C for 15 s, 68°C for 10 or 5 min (for *Lyst*-I and *Lyst*-II, respectively), followed by 20 or 10 min (for *Lyst*-I and *Lyst*-II, respectively) at 68°C. The same upstream primer (5′-AGCGGAGGTGAAGCCTTATGCTGAGACAGT-3′) was used for PCR amplification of both isoforms. Isoform-specific downstream primers used were 5′-TTATGTCCTGTGGGGACACTCCTTC-3′ (for *Lyst*-I) and 5′-ACAGAGCATCCCCACTTCCCTATCTAAAGT-3′ (for *Lyst*-II).

DNA sequencing and sequence analysis

PCR products were cloned using a TA cloning kit (Invitrogen Corporation, San Diego, CA) and both strands were cycle sequenced. The sequences were analyzed with the GCG Package (42) and searches of the National Center for Biotechnology Information database were performed using the BLAST network server (43) (National Library of Medicine, via INTERNET) and the Whitehead Institute Sequence Analysis Programs (MIT, Cambridge, MA).

Southern and Northern blot analysis

Preparation of mouse, human, bacteriophage P1 and yeast DNA samples, digestion with restriction endonucleases, agarose gel electrophoresis and Southern transfers were performed using standard techniques (44,45). An *Eco*RI monochromosomal somatic cell hybrid blot was obtained from BIOS Laboratories (New Haven, CT). Isolation of poly(A)$^+$ RNA from fibroblast and Epstein–Barr virus-transformed B lymphoblast cell lines, formaldehyde agarose gel electrophoresis and Northern blotting were performed according to standard procedures (44). A human RNA dot-blot containing poly(A)$^+$ RNA from 50 human adult and fetal tissues was obtained from Clontech Labs. The quantity of poly(A)$^+$ RNA on each dot was normalized for eight housekeeping genes, and varied from 100 to 500 ng. Membranes were hybridized with various *CHS* or actin probes labeled with [α-^{32}P] dCTP (45). Autoradiography or phosphorimaging was performed using X-ray film or a Molecular Dynamics phosphorimager (Sunnyvale, CA), respectively.

SSCP analysis

Detection of nucleotide changes by SSCP was performed as described by Orita *et al*. (46). Briefly, each PCR product was mixed with an equal volume of denaturing buffer and heated to 95°C for 3 min, after which the samples were loaded onto 0.8 mm thick, 10% native polyacrylamide gels. Gels were run at ambient temperature at 9 W for 6–10 h, depending on the size of the PCR product. Bands were visualized by silver staining (47). Primer sequences are available upon request.

Allele-specific oligonucleotide analysis

PCR products spanning the mutation site in patient 371 were transferred to nylon membranes using a slot-blot apparatus. Approximately 5 ng of each PCR product was treated with a denaturing solution (0.5 M NaOH, 1.5 M NaCl), split in half and loaded in duplicate. Two 17mer oligonucleotides were synthesized that span the region containing the mutation. One contained the sequence of the normal allele (5′-CGCACATGGCAACCCTT-3′), while the other contained the sequence of the mutant allele (5′-GCACATGGGCAACCCTT-3′). These were end-labeled with [γ-^{32}P] dATP using T4 polynucleotide kinase and hybridized to the membranes at 50°C. Hybridization and wash buffers were as described (48). Membranes were washed sequentially at 45, 55 and 65°C for 10 min each and exposed to X-ray film.

Acknowledgments

We thank K. Achey and S. Certain for technical assistance and Dr Seth Orlow for provision of mouse melanocyte RNA. We thank Dr Roberto Solari and Dr Charlie Hodgman for sequence alignments. S.F.K. is supported by the American Cancer Society, the Arthritis Foundation, Glaxo-Wellcome Research and Development, the Howard Hughes Medical Institute and the National Institutes of Health (AI39651 and AI39824). S.J.B. is supported by the Vanderbilt Cancer Center and the National Institutes of Health (5P30-AR 41943). G.S.B. is supported by grants from INSERM, l'Association Vaincre les Maladies Lysosomiales, l'Association Française contre les Myopathies, le Ministère de l'Education Nationale de l'Enseignement Supérieur et de la Recherche and l'Assistance Publique Hôpitaux de Paris.

References

1. Goodrich KH, Holcombe RF. Genetic localization of the gene for Chediak–Higashi syndrome to human chromosome 1q and linkage to nidogen. FASEB J 1995;43:13a.
2. Barrat FJ, et al. Genetic and physical mapping of the Chediak–Higashi syndrome on chromosome 1q42–43. Am J Hum Genet 1996;59:625–632. [PubMed: 8751864]
3. Fukai K, et al. Homozygosity mapping of the gene for Chediak–Higashi syndrome to chromosome 1q42–q44 in a segment of conserved synteny that includes the mouse *beige* locus *(bg)*. Am J Hum Genet 1996;59:620–624. [PubMed: 8751863]
4. Beguez-Cesar A. Neutropenia cronica maligna familiar con granulaciones atipicas de los leucocitos. Bol Soc Cubana Pediatr 1943;15:900–922.
5. Blume RS, Bennett JM, Yankee RA, Wolff SM. Defective granulocyte regulation in the Chediak–Higashi syndrome. N Engl J Med 1968;279:1009–1015. [PubMed: 5681251]
6. Wolff SM, Dale DC, Clark RA, Root RK, Kimball HR. The Chediak–Higashi syndrome: studies of host defenses. Ann Intern Med 1972;76:293–306. [PubMed: 4550589]
7. Blume RS, Wolff SM. The Chediak–Higashi syndrome: studies in four patients and a review of the literature. Med Baltimore 1972;51:247–280.
8. Root RK, Rosenthal AS, Balestra DJ. Abnormal bactericidal, metabolic and lysosomal functions of Chediak–Higashi syndrome leukocytes. J Clin Invest 1972;51:649–665. [PubMed: 4400956]
9. Roder JC, Haliotis T, Laing L, Kozbor D, Rubin P, Pross H, Boxer LA, White JG, Fauci AS, Mostowski H, Matheson DS. Further studies of natural killer cell function in Chediak–Higashi patients. Immunology 1982;46:555–560. [PubMed: 6212535]
10. Baetz K, Isaaz S, Griffiths GM. Loss of cytotoxic T lymphocyte function in Chediak–Higashi syndrome arises from a secretory defect that prevents lytic granule exocytosis. J Immunol 1995;154:6122–6131. [PubMed: 7751653]

11. Windhorst DB, Zelickson AS, Good RA. A human pigmentary dilution based on a heritable subcellular structural defect—the Chediak–Higashi syndrome. J Invest Dermatol 1968;50:9–18. [PubMed: 4169890]
12. Meyers KM, Stevens DR, Padgett GA. A platelet serotonin anomaly in the Chediak–Higashi syndrome. Res Commun Chem Pathol Pharmacol 1974;7:375–380. [PubMed: 4818380]
13. Maeda K, Sueishi K, Lida M. A case report of Chediak–Higashi syndrome complicated with systemic amyloidosis and olivocerebellar degeneration. Pathol Res Pract 1989;185:231–237. [PubMed: 2798223]
14. Pettit RE, Berdal KG. Chediak–Higashi syndrome. Neurologic appearance. Arch Neurol 1984;41:1001–1002. [PubMed: 6477224]
15. Misra VP, King RH, Harding AE, Muddle JR, Thomas PK. Peripheral neuropathy in the Chediak–Higashi syndrome. Acta Neuropathol Berl 1991;81:354–358. [PubMed: 2058369]
16. Brandt EJ, Elliott RW, Swank RT. Defective lysosomal enzyme secretion in kidneys of Chediak–Higashi (beige) mice. J Cell Biol 1975;67:774–788. [PubMed: 408]
17. Burkhardt JK, Wiebel FA, Hester S, Argon Y. The giant organelles in *beige* and Chediak–Higashi fibroblasts are derived from late endosomes and mature lysosomes. J Exp Med 1993;178:1845–1856. [PubMed: 7902407]
18. Zhao H, Boissy YL, Abdel-Malek Z, King RA, Nordlund JJ, Boissy RE. On the analysis of the pathophysiology of Chediak–Higashi syndrome. Defects expressed by cultured melanocytes. Lab Invest 1994;71:25–34. [PubMed: 8041115]
19. Griffiths GM. Secretory lysosomes—a special mechanism of regulated secretion in haemopoietic cells. Trends Cell Biol 1996;6:329–332. [PubMed: 15157429]
20. Barbosa MDFS, Nguyen QA, Tchernev VT, Ashley JA, Detter JC, Blaydes SM, Brandt SJ, Chotai D, Hodgman C, Solari RCE, Lovett M, Kingsmore SF. Identification of the homologous beige and Chediak–Higashi syndrome genes. Nature 1996;382:262–265. [PubMed: 8717042]
21. Perou CM, et al. Identification of the murine *beige* gene by YAC complementation and positional cloning. Nature Genet 1996;13:303–308. [PubMed: 8673129]
22. Kingsmore SF, Barbosa MDFS, Tchernev VT, Detter JC, Lossie AC, Seldin MF, Holcombe RF. Positional cloning of the Chediak–Higashi syndrome gene: genetic mapping of the *beige* locus on mouse chromosome 13. J Invest Med 1996;44:454–461.
23. Penner JD, Prieur DJ. Interspecific genetic complementation analysis with fibroblasts from humans and four species of animals with Chediak–Higashi syndrome. Am J Med Genet 1987;28:455–470. [PubMed: 3322007]
24. Perou C, Justice MJ, Pryor RJ, Kaplan J. Complementation of the beige mutation in cultured cells by episomally replicating murine yeast artificial chromosomes. Proc Natl Acad Sci USA 1996;93:5905–5909. [PubMed: 8650191]
25. Nagle DL, et al. Identification and mutation analysis of the complete gene for Chediak–Higashi syndrome. Nature Genet 1996;14:307–311. [PubMed: 8896560]
26. Kingsmore SF, Barbosa MDFS, Nguyen QA, Ashley JA, Blaydes SM, Tchernev VT, Detter JC, Lovett M. Physical mapping of the beige critical region on mouse chromosome 13. Mamm Genome 1996;7:773–775. [PubMed: 8854868]
27. Myers SM, Eng C, Ponder BAJ, Mulligan LM. Characterization of *RET* photo-oncogene 3′ splicing variants and polyadenylation sites: a novel C-terminus for RET. Oncogene 1995;11:2039–2045. [PubMed: 7478523]
28. Sugimoto Y, Kusakabe T, Kai T. Analysis of the *in vitro* translation product of a novel-type *Drosophila melanogaster* aldolase mRNA in which two carboxyl-terminal exons remain unspliced. Arch Biochem Biophys 1995;323:361–366. [PubMed: 7487099]
29. Sygiyama T, Nishio Y, Kishimoto T, Akira S. Identification of alternative splicing form of Stat2. FEBS Lett 1996;381:191–194. [PubMed: 8601453]
30. Zhao W, Manlley JL. Complex alternative RNA processing generates an unexpected diversity of poly (A) polymerase forms. Mol Cell Biol 1996;16:2378–2386. [PubMed: 8628305]
31. Van De Wetering M, Castrop J, Koriinev V, Clevers H. Extensive alternative splicing and dual promoter usage generate Tcf-1 protein isoforms with differential transcription control properties. Mol Cell Biol 1996;16:745–752. [PubMed: 8622675]

32. Lambright DG, Sondek J, Bohm A, Skiba NP, Hamm HE, Sigler PB. The 2.0 Å crystal structure of a heterotrimeric G protein. Nature 1996;379:311–319. [PubMed: 8552184]
33. Sobel A. Stathmin: a relay phosphoprotein for multiple signal transduction? Trends Biochem Sci 1991;16:301–305. [PubMed: 1957351]
34. Belmont LD, Mitchison TJ. Identification of a protein that interacts with tubulin dimers and increases the catastrophe rate of microtubules. Cell 1996;84:623–631. [PubMed: 8598048]
35. Marklund U, Larsson N, Gradin HM, Brattsand G, Gullberg M. Oncoprotein 18 is a phosphorylation-responsive regulator of microtubule dynamics. EMBO J 1996;15:5290–5298. [PubMed: 8895574]
36. Oliver JM, Zurier RB, Berlin RD. Concanavalin A cap formation on polymorphonuclear leukocytes of normal and beige (Chediak–Higashi) mice. Nature 1975;253:471–473. [PubMed: 163013]
37. Matteoni R, Kreis TE. Translocation and clustering of endosomes and lysosomes depends on microtubules. J Cell Biol 1987;105:1253–1265. [PubMed: 3308906]
38. Swanson JA, Bushnell A, Silverstein SC. Tubular lysosome morphology and distribution within macrophages depend upon the integrity of cytoplasmic microtubules. Proc Natl Acad Sci USA 1987;84:1921–1925. [PubMed: 3550801]
39. Swanson JA, Locke A, Ansel P, Hollenbeck PJ. Radial movement of lysosomes along microtubules in permealized macrophages. J Cell Sci 1992;103:210–209.
40. Oka JA, Weigel PH. Microtubule-depolymerizing agents inhibit asialo-orosomucoid delivery to lysosomes but not its endocytosis or degradation in isolated rat hepatocytes. Biochim Biphys Acta 1983;763:368–376.
41. Yamashita T, Wu N, Kupfer G, Corless C, Joenje H, Grompe M, D'Andrea AD. Clinical variability of Fanconi anemia (Type C) results from expression of an amino terminal truncated Fanconi anemia complementation group C polypeptide with partial activity. Blood 1996;87:4424–4432. [PubMed: 8639804]
42. Devereux J, Haeberli M, Smithies O. A comprehensive set of sequence analysis programs for the VAX. Nucleic Acids Res 1984;12:387–395. [PubMed: 6546423]
43. Altschul SF, Gish W, Miller H, Myers EW, Lipman DJ. Basic local alignment search tool. J Mol Biol 1990;215:403–410. [PubMed: 2231712]
44. Maniatis, T.; Fritsch, EF.; Sambrook, J. Moleular Cloning: A Laboratory Manual. Cold Spring Harbor Laboratory Press; Cold Spring Harbor, NY: 1982.
45. Barbosa MDF, Johnson SA, Achey K, Gutierrez MJ, Wakeland EK, Zerial M, Kingsmore SF. The rab protein family: genetic mapping of six *Rab* genes in the mouse. Genomics 1995;30:439–444. [PubMed: 8825628]
46. Orita M, Suzuki Y, Sekiya T, Hayashi K. Rapid and sensitive detection of point mutations and DNA polymorphisms using the polymerase chain reaction. Genomics 1989;5:874–879. [PubMed: 2687159]
47. Beidler JL, Hilliard PR, Rill RL. Ultrasensitive staining of nucleic acids with silver. Anal Biochem 1982;126:374–380. [PubMed: 6186158]
48. Church GM, Gilbert W. Genomic sequencing. Proc Natl Acad Sci USA 1984;81:1991–1995. [PubMed: 6326095]

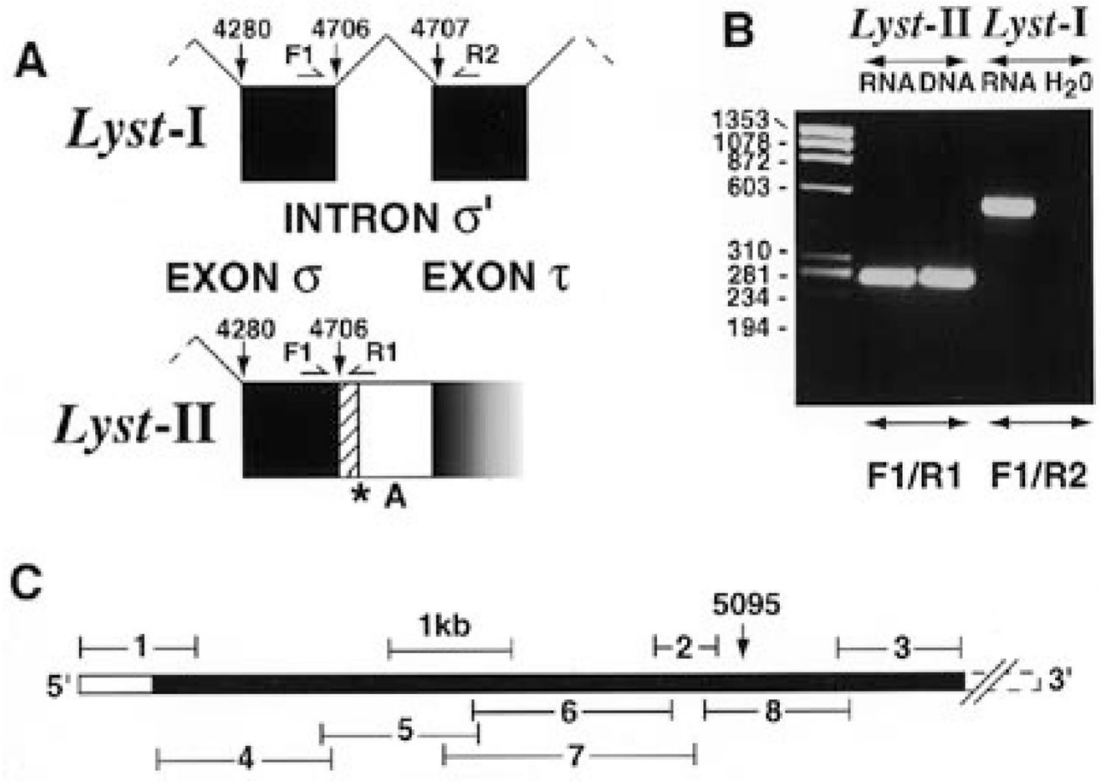

Figure 1.

cDNA structures and alternative splicing of the Chediak–Higashi syndrome gene. (**A**) Alternative splicing of the mouse *bg* gene (*Lyst)*. Solid boxes represent *Lyst* exons σ and τ (not drawn to scale). Splicing of exon σ to exon τ occurs in the *Lyst*-I mRNA (~12 kb). The hatched box represents the intronic region that forms the 3′ end of the *Lyst*-II ORF (5.9 kb). The intron contains a stop codon (*) and a polyadenylation signal (A). Nucleotide positions indicated are from GenBank accession No. L77884 (*Lyst*-II) and U70015 (*Lyst*-I). (**B**) Detection of mRNA isoforms of the mouse *bg* gene by RT-PCR and genomic PCR. DNase-treated mouse melanocyte RNA was reverse transcribed and amplified with primers F1/R1 (expected amplicon size 273 bp) or F1/R2 (expected amplicon size 560 bp). RNase-treated C57BL/6J DNA was amplified with primers F1/R1. The primer sequences are F1, 5′-TGTGGAATACATCCAATGAATCCGAGAGTGC-3′;F2, 5′-GAGCCAAGAAAGAGGCTGAT-3′; R1, 5′-GGTTTCGGACTCAAAAGTTTGTCGGAACTT-3′; R2, 5′-GAGACCCATATGGAGATTTC-3′. (**C**) Schematic representation of PCR clones corresponding to the human *CHS* cDNA (GenBank accession No. U70064). The solid and open bars represent the *CHS* coding region and the 5′ UTR, respectively. Nucleotide 5095 corresponds to the junction between the largest isoform (*CHS*-I, shown), and the smaller isoform (*CHS*-II) that arises through retention of intron σ′. The three human ESTs identified by database searches with the mouse sequence (#1, #2 and #3; GenBank accession Nos: #1, L77889; #2, W26957; #3, H51623) are shown at the top. Clones #4, #5, #6 and #8 are RT-PCR products. Clone #7 is a 2 kb 5′RACE product.

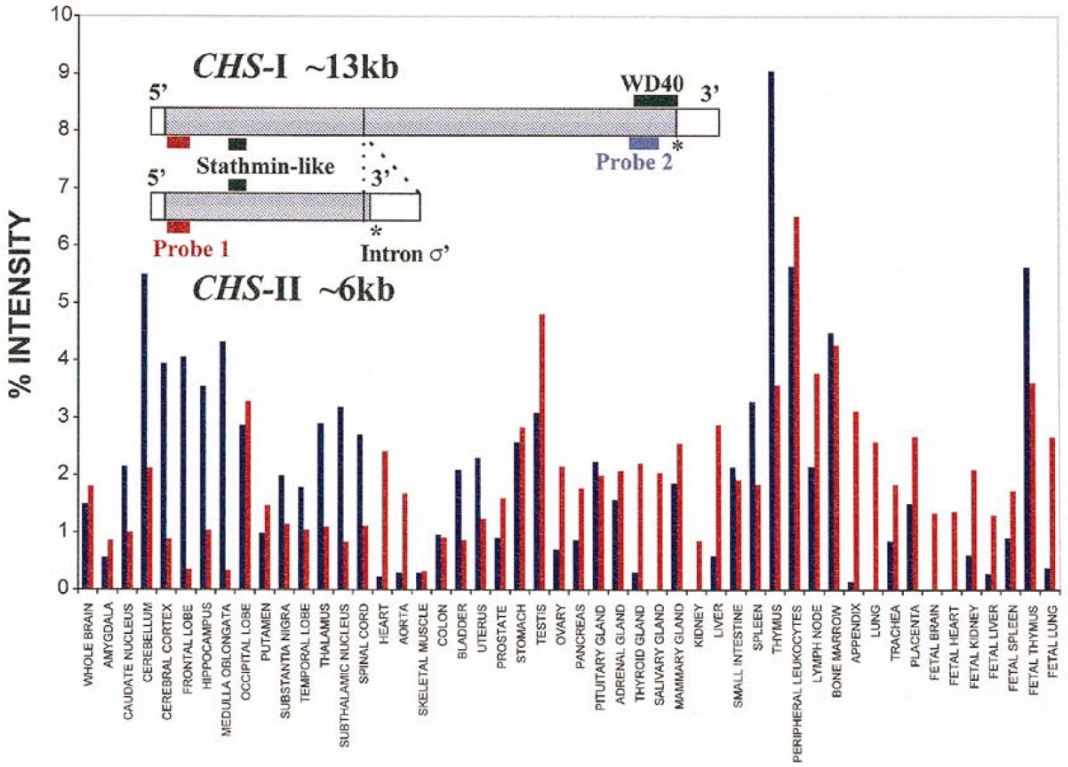

Figure 2.

Comparison of the relative abundance of *CHS* mRNA isoforms in human tissues after normalization. The inset shows the human 5.8 kb cDNA isoform (*CHS*-II, which arises through incomplete splicing, with intron σ′ supplying the 3′ end of the transcript), the largest cDNA (*CHS*-I, 13.5 kb, which results from removal of intron σ′) and the locations of probes. A normalized human RNA dot-blot was hybridized sequentially with a cDNA probe specific for the largest isoform (shown in blue, nucleotides 10941–11590 of human *CHS*, GenBank accession No. U67615) and a cDNA probe that identifies all *CHS* transcripts (shown in orange, nucleotides 190–445 of human *CHS*, GenBank accession Nos U70064 and U84744) (20,25). Variation of relative mRNA abundance among tissues was assessed by phosphorimaging, dot quantitation, subtraction of background and calculation of the intensity percentage for each tissue. The relative mRNA abundances between normalized tissues for each probe were expressed as the percentage of the total hybridization signal obtained for each tissue with that probe. The average percentage intensity for housekeeping genes in all tissues was ~2% (data not shown). No hybridization was evident to control dots containing yeast total RNA, yeast tRNA, *E.coli* rRNA, *E.coli* DNA, poly r(A), human C_0t1 DNA and human DNA (data not shown). Exposure time for phosphorimaging was 20 h.

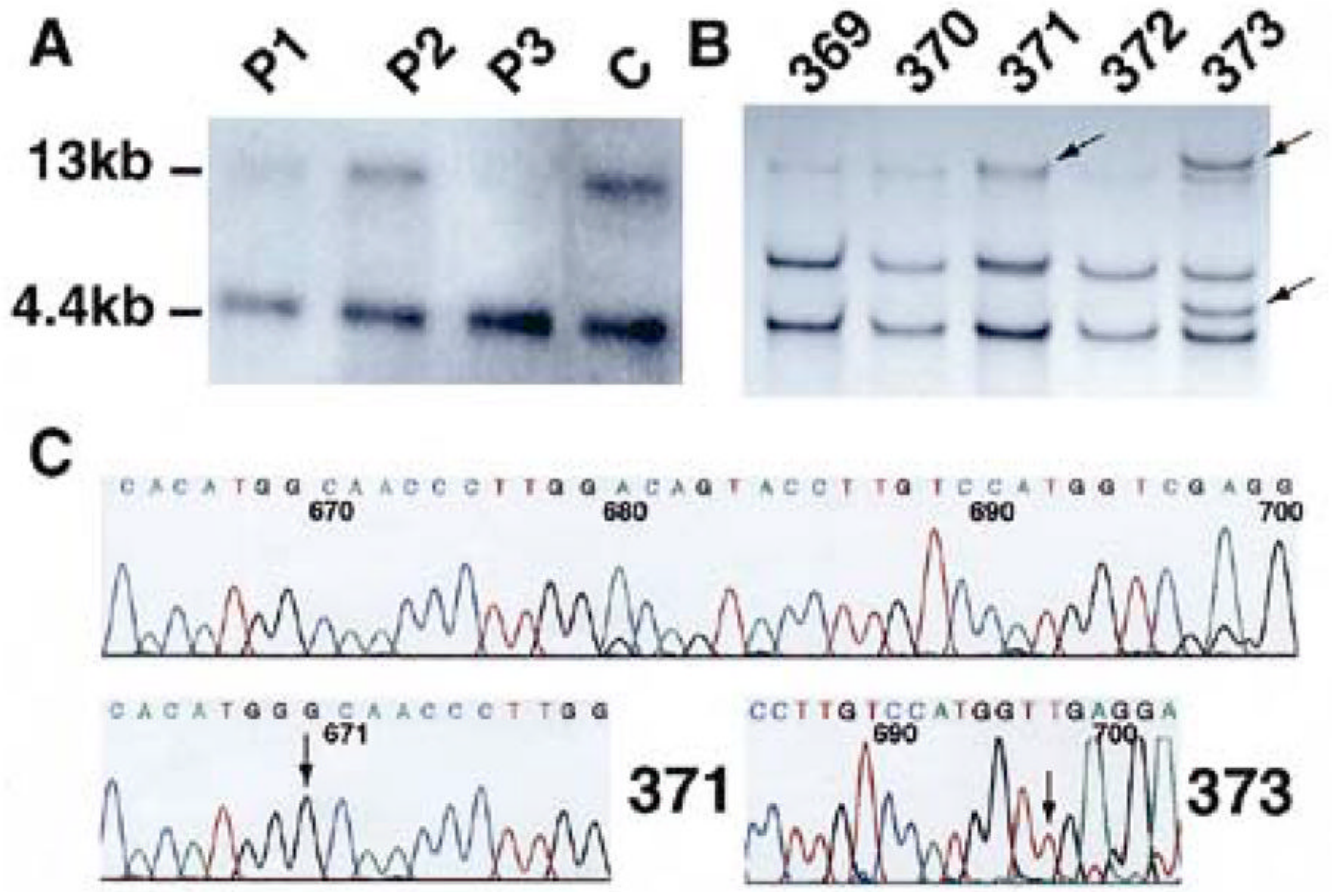

Figure 3.

Mutation analysis in CHS patients. (**A**) A Northern blot of 2 μg aliquots of lymphoblastoid poly(A)$^+$ RNA from CHS patients and a control. The probe used for hybridization corresponds to nucleotides 490–817 of the *CHS* cDNA (GenBank accession No. U70064). Exposure time for autoradiography was 48 h. (**B**) SSCP analysis of cDNA corresponding to nucleotides 439–806 of the *CHS* cDNA. Each lane contains samples from individual patients as indicated. Extra bands in lanes corresponding to patients 371 and 373 are denoted with an arrow. (**C**) Sequence chromatograms showing mutations in cDNA clones from patients 371 and 373. The upper part is normal human *CHS* cDNA sequence. The arrows indicate the positions of a G insertion (coding domain nucleotide 118, patient 371) and C→T substitution (coding domain nucleotide 148, patient 373). The sense strand is shown.

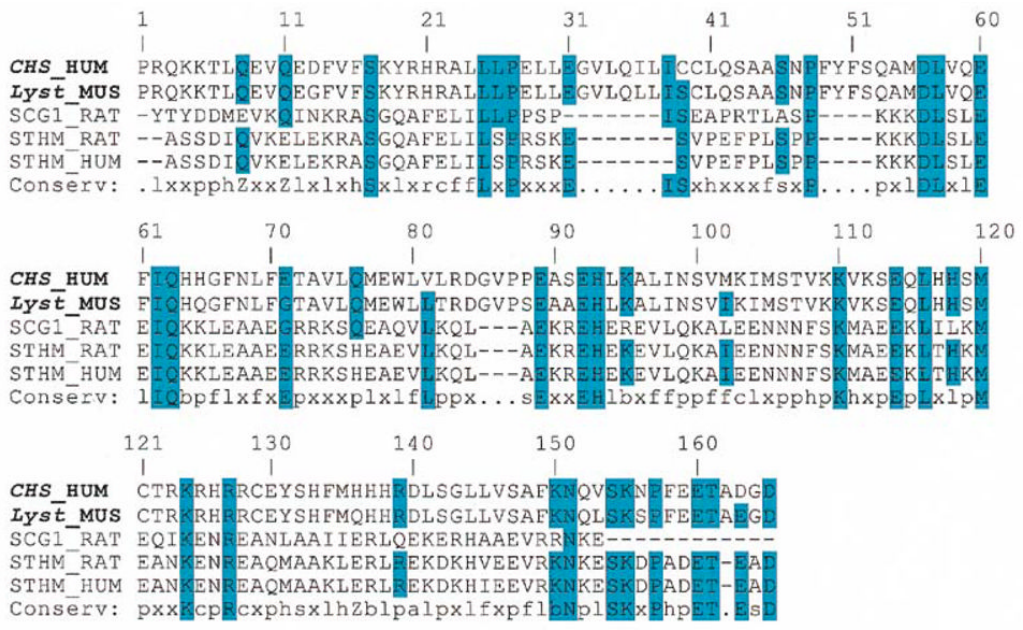

Figure 4.

Multiple alignment of the stathmin-like region of the human and mouse CHS proteins (CHS_HUM, Lyst_MUS) with human and rat stathmins and rat SCG10 (STHM_HUM, STHM_RAT and SCG1_RAT, respectively) as generated by Clustalw. The extent of conservation with the stathmin family is shown below the alignment. Where residues are totally conserved, they are noted on this line, and Z refers to Glu or Gln. Otherwise, a, b, c, f, h, l, p, r and s respectively refer to acidic, basic, charged, aliphatic, hydrophobic, large, polar, aromatic and small amino acid groups respectively. A dot indicates an insertion in the *CHS* gene sequence. An x indicates a residue that is not conserved.

Table 1

Mutations identified in CHS patients

Patient	Zygosity	Mutation[a]	Consequence
P1	?	?	↓↓ 13.5 kb mRNA
P3	?	?	↓↓ 13.5 kb mRNA
369	Heterozygous	bp 3073 + 3074 deleted	Codon 1026 frameshift; stop @ codon 1030
370	Homozygous	C3085T	Q 1029 X
371	Heterozygous	G insertion @ bp 118	Codon 40 frameshift; stop @ codon 62
373	Heterozygous	C148T	R 50 X

[a] Nucleotide positions of mutations within the coding domain of *CHS*.